Acta Crystallographica Section C
Crystal Structure Communications
ISSN 0108-2701

Coordination and hydrogen-bonding assemblies in hybrid reaction products between 5,10,15,20-tetra-4-pyridylporphyrin and dysprosium trinitrate hexahydrate

Sophia Lipstman and Israel Goldberg*

School of Chemistry, Sackler Faculty of Exact Sciences, Tel-Aviv University, Ramat-Aviv, 69978 Tel-Aviv, Israel
Correspondence e-mail: goldberg@post.tau.ac.il

Received 23 June 2010
Accepted 7 July 2010
Online 14 July 2010

Reactions of the title free-base porphyrin compound (TPyP) with dysprosium trinitrate hexahydrate in different crystallization environments yielded two solid products, *viz.* [μ-5,15-bis(pyridin-1-ium-4-yl)-10,20-di-4-pyridylporphyrin]bis[aquatetranitratodysprosium(III)] benzene solvate, $[Dy_2(NO_3)_8(C_{40}H_{28}N_8)(H_2O)_2]\cdot C_6H_6$, (I), and 5,10,15,20-tetrakis(pyridin-1-ium-4-yl)porphyrin pentaaquadinitratodysprosate(III) pentanitrate diethanol solvate dihydrate, $(C_{40}H_{30}N_8)[Dy(NO_3)_2(H_2O)_5](NO_3)_5\cdot 2C_2H_6O\cdot 2H_2O$, (II). Compound (I) represents a 2:1 metal–porphyrin coordinated complex, which lies across a centre of inversion. Two *trans*-related pyridyl groups are involved in Dy coordination. The two other pyridyl substituents are protonated and involved in intermolecular hydrogen bonding along with the metal-coordinated water and nitrate ligands. Compound (II) represents an extended hydrogen-bonded assembly between the tetrakis(pyridin-1-ium-4-yl)porphyrin tetracation, the $[Dy(NO_3)_2(H_2O)_5]^+$ cation and the free nitrate ions, as well as the ethanol and water solvent molecules. This report provides the first structural characterization of the exocyclic dysprosium complex with tetrapyridylporphyrin. It also demonstrates that charge balance can be readily achieved by protonation of the peripheral pyridyl functions, which then enhances their capacity in hydrogen bonding as H-atom donors rather than H-atom acceptors.

Comment

The tetra-4-pyridylporphyrin ligand (TPyP) is characterized by rigid square-planar geometry, bears multiple diverging molecular recognition sites for metal coordination as well as hydrogen bonding, and consequently reveals an extraordinarily rich supramolecular chemistry. Of particular interest is the coordination polymerization of this scaffold through exocyclic metal ion connectors. A survey of the literature indicates that the TPyP moiety provides an excellent building block for the formation of extended hybrid coordination polymers of diverse topologies when reacted with exocyclic transition metal ion connectors such as Ag^I (*e.g.* Carlucci *et al.*, 2003), Cd^{II} (*e.g.* Zheng *et al.*, 2007), Cu^{II} (*e.g.* Ohmura *et al.*, 2006), Fe^{II} (Hagrman *et al.*, 1999), Hg^{II} and Pb^{II} (Sharma *et al.*, 1999) ions. Structures with exocyclic coordination to the TPyP macrocycle of selected transition metals in discrete complexes have been reported as well (*e.g.* Kon *et al.*, 2006). A few coordination polymers and molecular complexes of lanthanoid (Ln) ions with simple bipyridyl ligands are known (Sharma & Rogers, 1999, and references therein), but analogous compounds with the TPyP unit have not been explored until recently. This could be due to the oxophilic nature of the lanthanoid ions and their much lower tendency to coordinate with aromatic pyridyl sites.

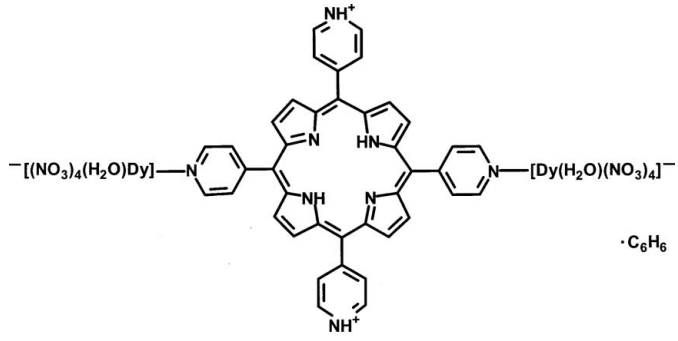

(I)

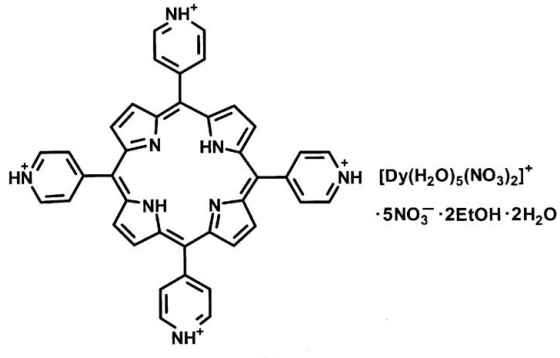

(II)

In recent studies, newer types of framework solids were obtained (Lipstman & Goldberg, 2010) by reacting TPyP with various aqua nitrate salts of lanthanoid *f*-metals. Those materials are characterized by open architectures of three-dimensional connectivity, which are sustained either by a combination of coordination polymerization in one direction and hydrogen bonding in the other directions, or by hydrogen-bonding interactions between the organic and inorganic components in all three dimensions. Direct coordination bonding between a lanthanoid ion and the pyridyl sites of TPyP has been observed thus far for La, Nd, Sm, Gd and Tb ions in their 3+ oxidation state (Lipstman & Goldberg, 2009, 2010). Direct insertion of the lanthanoids into the centre of the porphyrin core is unlikely due to the relatively large size of

  doi:10.1107/S0108270110026892

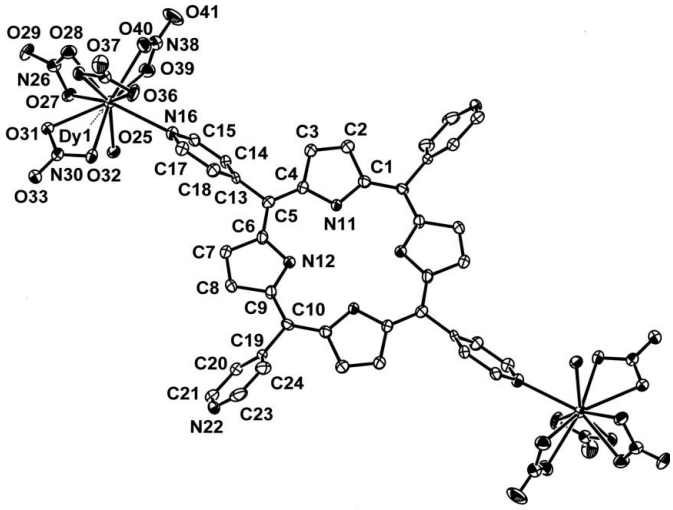

Figure 1
The molecular structure of compound (I), showing the atom-labelling scheme. Molecules of this complex are located across centres of inversion, and only the unique atoms of the asymmetric unit are labelled. Ellipsoids represent displacement parameters at the 50% probability level at *ca* 110 K. The H atoms and the disordered benzene solvent molecules have been omitted.

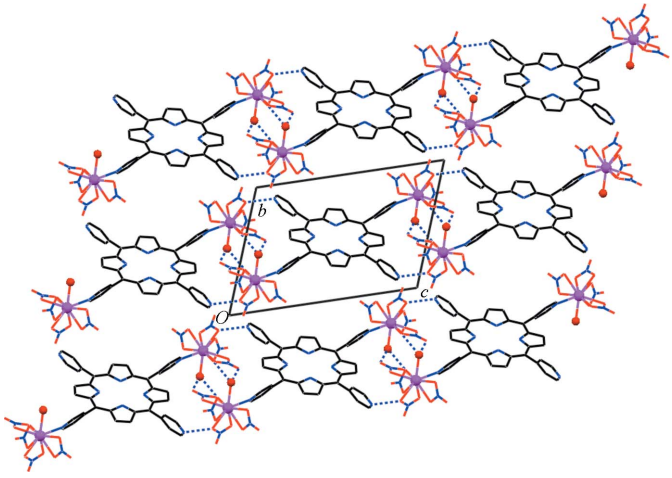

Figure 2
The crystal packing of (I), projected down the *a* axis of the unit cell. Note the separate columns of the organic and inorganic components of this structure. The intermolecular hydrogen bonds are depicted by dashed lines. Only the Dy ions and the coordinated water ligand are shown as small spheres; the remainder of the illustration is shown in wireframe. The benzene solvent molecules located on, and disordered about, the inversion centre at (0, 0, $\frac{1}{2}$) have been omitted (see *Experimental*).

these ions. The ionic radii along the lanthanide series La^{III} to Lu^{III} vary from 1.03 to 0.86 Å (Cotton, 2006), as compared, for example, to the ionic radius of 0.74 Å for Zn^{II} that fits just perfectly into the porphyrin macrocycle. Only a small number of double-decker-type compounds in which the Ln ions are sandwiched between, and coordinated by, the central pyrrole rings of two TPyPs has been observed (Ikeda *et al.*, 2000).

Within the context of our continuing investigations on porphyrin framework solids (Goldberg, 2008) and on the supramolecular hybrid assemblies of the TPyP with Ln ions,

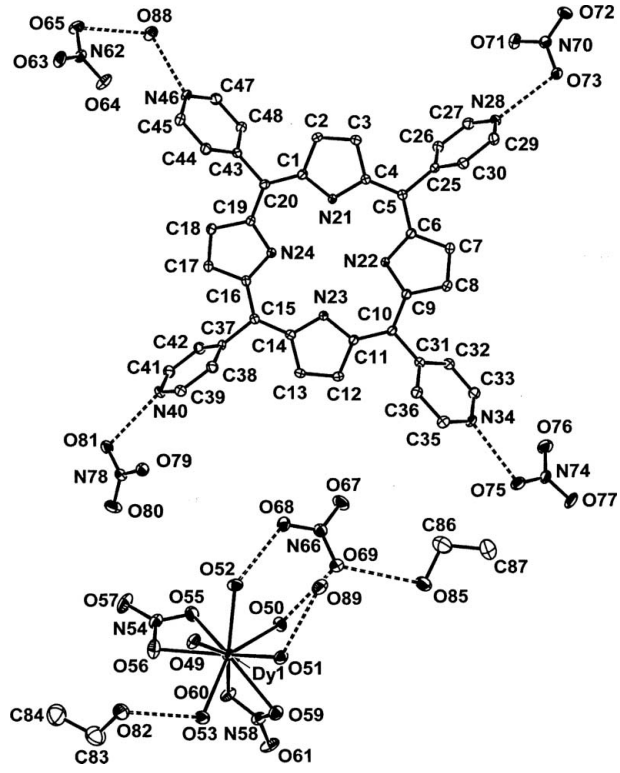

Figure 3
The molecular structure of compound (II), showing the atom-labelling scheme. Ellipsoids represent displacement parameters at the 50% probability level at *ca* 110 K. H atoms have been omitted. In order to avoid severe overcrowding, the upper and lower parts of this figure were drawn and labelled separately; as a result the Figure does not represent their relative orientations in the crystal. Consequently, only hydrogen bonds between the component species within each part are shown (dashed lines); all hydrogen-bond interactions are listed in Table 4.

we describe here the structures of two new solid products, (I) and (II), obtained by reacting the porphyrin ligand with dysprosium nitrate hexahydrate, $Dy^{III}(NO_3)_3{\cdot}6H_2O$, under different crystallization conditions. It should be noted (see *Experimental*) that the large excess of the aqua nitrate salt in the reaction creates acidic conditions which promote protonation of the TPyP Lewis base, accompanied by insertion of additional nitrate ions into the solid products. This has been observed in earlier studies of the tetranitratolanthanide complexes with TPyP (Lipstman & Goldberg, 2009, 2010), as well as with 4,4′-bipyridine (Sharma & Rogers, 1999). Compound (I) provides another example of this. Here, two *trans*-related pyridyl groups of the TPyP component become protonated, while the other two pyridyl functions engage in coordinative bonds with two Dy metal centres. The structure of this product, $(TPyPH_2)[Dy(NO_3)_4(H_2O)]_2$, is illustrated in Fig. 1. The porphyrin core in the formed metallo-organic complex is essentially planar. The Dy^{III} ion is coordinated by four chelating nitrate ions and by one water molecule (Table 1), being thus characterized by a coordination number of 9 (typical of Ln metal ions in their most common oxidation state of 3+). The crystal packing of (I) involves hydrogen-bonding interactions between neighbouring units of the

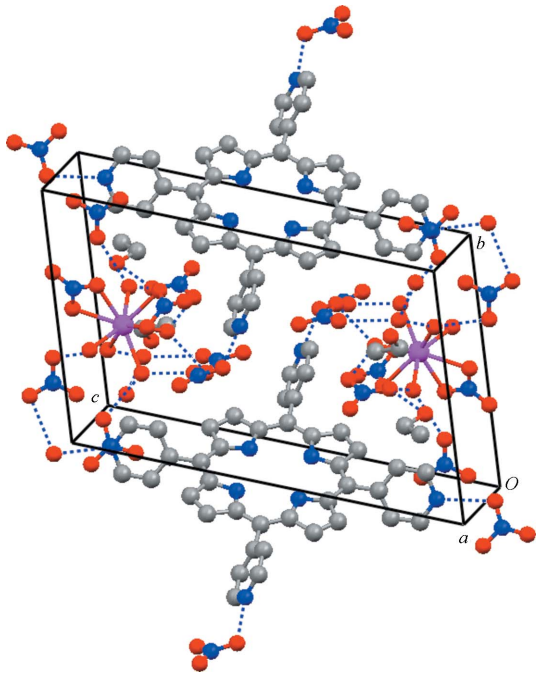

Figure 4
Ball-and-stick representation of the crystal packing in (II), with dashed lines indicating the hydrogen bonding between the component species. Note the segregation between the porphyrin and the Dy complex zones in the crystal. H atoms have been omitted.

complex, utilizing the water ligand and pyridinium fragments as H-atom donors and the metal-coordinated nitrate ions as H-atom acceptors (Table 2). It reveals columnar organization of the organic and inorganic components along the *a* axis of the crystal (Fig. 2). The porphyrin entities are stacked along *a* in an offset-stacked manner, as commonly observed in a large variety of tetraarylporphyrin compounds (Byrn *et al.*, 1993, and references therein). The interstitial voids between the porphyrin columns entrap disordered molecules of the benzene crystallization solvent. The inorganic $[Dy(NO_3)_4(H_2O)]^-$ components displaced along the *a* axis at $(x, \frac{1}{2}, 0)$ are hydrogen bonded to one another across inversion centres at $(0, \frac{1}{2}, 0)$ and $(\frac{1}{2}, \frac{1}{2}, 0)$; the $(TPyPH_2)^{2+}$ entity located across the inversion centre at $(\frac{1}{2}, \frac{1}{2}, \frac{1}{2})$ takes part in hydrogen bonding with adjacent units of the coordination complex near the (1, 1, 0) and (0, 0, 1) corners of the unit cell (Table 2).

Under more acidic conditions, due to the presence of benzenetricarboxylic acid in the crystallization mixture, full protonation of the peripheral pyridyl groups of the TPyP has occurred in compound (II). Moreover, under such conditions the basic nitrate anions have a comparable tendency to be present in either a free or a metal-coordinated state, due to the competing ion-pairing and coordination interactions. In an aqueous protic environment, this also leads to crystallization of the product in a solvated form of complex composition: $(TPyPH_4)[Dy(NO_3)_2(H_2O)_5](NO_3)_5{\cdot}2EtOH{\cdot}2H_2O$ (Fig. 3). The Dy^{III} ion in (II) is also nine-coordinate, linking singly to five molecules of water and doubly to two nitrate ions (Table 3). Given the large number of potential O—H and N—H H-atom donor and the nitrate H-atom acceptor sites, the supramolecular organization in this structure involves a large number of O—H···O and N—H···O hydrogen bonds (Table 4). Fig. 4 illustrates the hydrogen-bonded crystal packing of (II). It also shows that the protonated pyridyl sites of the $(TPyPH_4)^{4+}$ residue are not available for metal coordination, being involved in charge-assisted hydrogen bonds with the surrounding nitrate ions and water molecules. The conformation of the porphyrin macrocycle in (II) is essentially planar. The observed crystal packing exhibits segregated zones of the porphyrin and the metal-complex fragment parallel to the (*ac*) plane of the crystal, the former being centred at $y = 0$ and the latter clustering around $y = \frac{1}{2}$.

In summary, we report here on another example of previously rarely observed direct exocyclic coordination adducts of TPyP and Ln ions (Lipstman & Goldberg, 2009, 2010). Structures in which the TPyP entity is involved in supramolecular hydrogen bonding through their pyridyl groups are also scarce (Koner & Goldberg, 2009, 2010; Langford & Woodward, 2007; Kim *et al.*, 2005). While it is expected in crystal engineering that the pyridyl N-atom sites will normally engage in hydrogen bonds as H-atom acceptors with complementary H-atom donors, in structures (I) and (II) the protonated pyridyl sites adopt an opposite H-atom donating function.

Experimental

The porphyrin and lanthanoid salt reagents and all solvents were obtained commercially. Compound (I) was obtained by dissolving dysprosium(III) trinitrate hexahydrate (1.24 mmol) and TPyP (0.046 mmol) in a mixture of ethanol (6 ml) and 1,2-dichlorobenzene (8 ml). This solution was refluxed overnight and filtered. Then it was placed in a tube and covered carefully with a layer of benzene in order to induce crystallization of the product by slow diffusion of benzene into the mother solution. Purple prisms of the solid material, (I), were obtained after 5 months. Compound (II) was obtained under more acidic conditions by dissolving $Dy(NO_3)_3{\cdot}6H_2O$ (0.607 mmol), TPyP (0.026 mmol) and benzene-1,3,5-tricarboxylic acid (0.030 mmol) in a mixture of ethanol (12 ml) and 1,2-dichlorobenzene (12 ml). The resulting solution was refluxed for 12 h, filtered and left for crystallization by slow evaporation. Diffraction-quality crystals of (II) appeared at the bottom of the tube after 40 d.

Compound (I)

Crystal data

$[Dy_2(NO_3)_8(C_{40}H_{28}N_8)(H_2O)_2]{\cdot}C_6H_6$
$M_r = 1477.82$
Triclinic, $P\overline{1}$
$a = 7.7897$ (2) Å
$b = 12.2577$ (2) Å
$c = 17.2316$ (5) Å
$\alpha = 70.1447$ (10)°
$\beta = 89.341$ (1)°
$\gamma = 75.3827$ (16)°
$V = 1492.45$ (6) Å^3
$Z = 1$
Mo $K\alpha$ radiation
$\mu = 2.58$ mm^{-1}
$T = 110$ K
0.15 × 0.10 × 0.05 mm

Data collection

Nonius KappaCCD diffractometer
Absorption correction: multi-scan (Blessing, 1995)
$T_{min} = 0.699$, $T_{max} = 0.882$
13999 measured reflections
6457 independent reflections
5074 reflections with $I > 2\sigma(I)$
$R_{int} = 0.054$

Table 1
Selected bond lengths (Å) for (I).

Dy1—O25	2.355 (3)	Dy1—O35	2.462 (3)
Dy1—O39	2.406 (3)	Dy1—O31	2.462 (3)
Dy1—O28	2.434 (3)	Dy1—O27	2.582 (3)
Dy1—O40	2.439 (3)	Dy1—O36	2.613 (4)
Dy1—O32	2.451 (3)		

Table 2
Hydrogen-bond geometry (Å, °) for (I).

D—H···A	D—H	H···A	D···A	D—H···A
N22—H22···O35^{i}	0.88	2.26	2.926 (5)	132
O25—H25A···O27^{ii}	0.95	1.86	2.784 (4)	164
O25—H25B···O33^{iii}	0.95	1.83	2.762 (4)	168

Symmetry codes: (i) $-x+1, -y+1, -z$; (ii) $-x-1, -y+1, -z$; (iii) $-x, -y+1, -z$.

Refinement

$R[F^2 > 2\sigma(F^2)] = 0.042$	379 parameters
$wR(F^2) = 0.083$	H-atom parameters constrained
$S = 0.97$	$\Delta\rho_{max} = 1.36$ e Å^{-3}
6457 reflections	$\Delta\rho_{min} = -1.03$ e Å^{-3}

Compound (II)

Crystal data

$(C_{40}H_{30}N_8)[Dy(NO_3)_2(H_2O)_5](NO_3)_5{\cdot}2C_2H_6O{\cdot}2H_2O$	$\beta = 80.9684\ (8)^\circ$
$M_r = 1437.54$	$\gamma = 73.3707\ (7)^\circ$
Triclinic, $P\overline{1}$	$V = 2811.52\ (8)$ Å^3
$a = 12.8961\ (2)$ Å	$Z = 2$
$b = 12.9222\ (2)$ Å	Mo $K\alpha$ radiation
$c = 18.5978\ (3)$ Å	$\mu = 1.44$ mm^{-1}
$\alpha = 71.6843\ (7)^\circ$	$T = 110$ K
	$0.55 \times 0.10 \times 0.05$ mm

Data collection

Nonius KappaCCD diffractometer	47169 measured reflections
Absorption correction: multi-scan (Blessing, 1995)	13315 independent reflections
	11865 reflections with $I > 2\sigma(I)$
$T_{min} = 0.512$, $T_{max} = 0.932$	$R_{int} = 0.044$

Refinement

$R[F^2 > 2\sigma(F^2)] = 0.034$	813 parameters
$wR(F^2) = 0.082$	H-atom parameters constrained
$S = 1.04$	$\Delta\rho_{max} = 2.00$ e Å^{-3}
13315 reflections	$\Delta\rho_{min} = -1.62$ e Å^{-3}

H atoms bound to C atoms were located in calculated positions and were constrained to ride on their parent atoms, with C—H distances of 0.95 and 0.98 Å and with U_{iso}(H) = 1.2 or 1.5U_{eq}(C). Those bound to O and N atoms were either located in difference Fourier maps or placed in calculated positions to correspond to idealized hydrogen-bonding geometries, with O—H and N—H distances within the ranges 0.83–1.03 and 0.85–0.96 Å, respectively. Their atomic positions were not refined, and they were constrained to ride on their parent atoms, with U_{iso}(H) = 1.5U_{eq}(carrier). In (I), the benzene crystallization solvent trapped in the crystal lattice was found to be severely disordered such that it could not be reliably modelled as discrete atoms. It is located on, and disordered about, the centre of inversion at (0, 0, $\frac{1}{2}$). For the final refinement, its contribution to the diffraction pattern was subtracted using the SQUEEZE procedure in *PLATON* (Spek, 2009). In (II), the two H atoms bound to N atoms within the porphyrin core could not be located reliably. As some residual electron density was observed near all the pyrrole N atoms, the H atoms bound to them were assumed to be disordered between the four pyrrole rings, and accordingly they were placed in calculated positions, with N—H distances of 0.88 Å and with U_{iso}(H) = 1.2U_{eq}(N).

Table 3
Selected bond lengths (Å) for (II).

Dy1—O51	2.3172 (18)	Dy1—O49	2.4280 (18)
Dy1—O50	2.3532 (17)	Dy1—O56	2.4372 (19)
Dy1—O53	2.3582 (18)	Dy1—O55	2.507 (2)
Dy1—O52	2.3802 (18)	Dy1—O59	2.5196 (19)
Dy1—O60	2.4185 (19)		

Table 4
Hydrogen-bond geometry (Å, °) for (II).

D—H···A	D—H	H···A	D···A	D—H···A
N28—H28···O73	0.93	1.82	2.727 (3)	164
N34—H34···O75	0.89	1.88	2.743 (3)	162
N40—H40···O81	0.85	1.88	2.722 (3)	174
N46—H46···O88	0.96	1.87	2.749 (3)	150
O49—H49A···O75^{i}	0.83	1.96	2.776 (3)	167
O49—H49B···O79	0.91	1.87	2.744 (3)	159
O50—H50A···O69	0.92	1.86	2.748 (3)	163
O50—H50B···O63^{ii}	0.84	1.90	2.724 (3)	168
O51—H51A···O89	0.84	1.93	2.769 (3)	173
O51—H51B···O63^{iii}	0.91	1.82	2.726 (3)	174
O52—H52A···O72^{iv}	0.86	2.06	2.834 (3)	149
O52—H52B···O68	1.03	1.74	2.744 (3)	164
O53—H53A···O82	0.83	1.89	2.719 (3)	174
O53—H53B···O85^{i}	0.86	1.93	2.759 (3)	163
O82—H82···O80	0.92	2.17	3.011 (3)	151
O85—H85···O69	1.00	1.94	2.923 (3)	170
O88—H88A···O65	0.93	2.05	2.924 (3)	156
O88—H88B···O89^{v}	0.85	2.00	2.840 (3)	172

Symmetry codes: (i) $-x+1, -y-1, -z+2$; (ii) $x, y, z+1$; (iii) $-x+1, -y-1, -z+1$; (iv) $-x, -y, -z+1$; (v) $x, y+1, z-1$.

For both compounds, data collection: *COLLECT* (Nonius, 1999); cell refinement: *DENZO* (Otwinowski & Minor, 1997); data reduction: *DENZO*; program(s) used to solve structure: *SIR97* (Altomare *et al.*, 1994); program(s) used to refine structure: *SHELXL97* (Sheldrick, 2008); molecular graphics: *ORTEPIII* (Burnett & Johnson, 1996), *Mercury* (Macrae *et al.*, 2006); software used to prepare material for publication: *SHELXL97*.

This research was supported by the Israel Science Foundation (grant No. 502/08).

Supplementary data for this paper are available from the IUCr electronic archives (Reference: GD3355). Services for accessing these data are described at the back of the journal.

References

Altomare, A., Cascarano, G., Giacovazzo, C., Guagliardi, A., Burla, M. C., Polidori, G. & Camalli, M. (1994). *J. Appl. Cryst.* **27**, 435.
Blessing, R. H. (1995). *Acta Cryst.* A**51**, 33–38.
Burnett, M. N. & Johnson, C. K. (1996). *ORTEPIII*. Report ORNL-6895. Oak Ridge National Laboratory, Tennessee, USA.
Byrn, M. P., Curtis, C. J., Hsiou, Y., Khan, S. I., Sawin, P. A., Tendick, S. K., Terzis, A. & Strouse, C. E. (1993). *J. Am. Chem. Soc.* **115**, 9480–9497.
Carlucci, L., Ciani, G., Proserpio, D. M. & Porta, F. (2003). *Angew. Chem. Int. Ed.* **42**, 317–322.

Cotton, S. (2006). In *Lanthanide and Actinide Chemistry*. Chichester: Wiley.
Goldberg, I. (2008). *CrystEngComm*, **10**, 637–645.
Hagrman, D., Hagrman, P. J. & Zubieta, J. (1999). *Angew. Chem. Int. Ed.* **38**, 3165–3168.
Ikeda, M., Takeuchi, M., Sugasaki, A., Robertson, A., Imada, T. & Shinkai, S. (2000). *Supramol. Chem.* **12**, 321–345.
Kim, H.-J., Jo, H.-J., Kim, J., Kim, S.-Y., Kim, D. & Kim, K. (2005). *CrystEngComm*, **7**, 417–420.
Kon, H., Tsuge, K., Imamura, T., Sasaki, Y., Ishizaka, S. & Kitamura, N. (2006). *Inorg. Chem.* **45**, 6875–6883.
Koner, R. & Goldberg, I. (2009). *CrystEngComm*, **11**, 1217–1219.
Koner, R. & Goldberg, I. (2010). *J. Incl. Phenom. Macrocycl. Chem.* **66**, 403–408.
Langford, S. J. & Woodward, C. P. (2007). *CrystEngComm*, **9**, 218–221.
Lipstman, S. & Goldberg, I. (2009). *Acta Cryst.* C**65**, m371–m373.
Lipstman, S. & Goldberg, I. (2010). *Cryst. Growth Des.* **10**, 1823–1832.
Macrae, C. F., Edgington, P. R., McCabe, P., Pidcock, E., Shields, G. P., Taylor, R., Towler, M. & van de Streek, J. (2006). *J. Appl. Cryst.* **39**, 453–457.
Nonius (1999). *COLLECT*. Nonius BV, Delft, The Netherlands.
Ohmura, T., Usaki, A., Fukumori, K., Ohta, T., Ito, M. & Tatsumi, K. (2006). *Inorg. Chem.* **45**, 7988–7990.
Otwinowski, Z. & Minor, W. (1997). *Methods in Enzymology*, Vol. 276, *Macromolecular Crystallography*, Part A, edited by C. W. Carter Jr & R. M. Sweet, pp. 307–326. New York: Academic Press.
Sharma, C. V. K., Broker, G. A., Huddleston, J. G., Baldwin, J. W., Metzger, R. M. & Rogers, R. D. (1999). *J. Am. Chem. Soc.* **121**, 1137–1144.
Sharma, C. V. K. & Rogers, R. D. (1999). *Chem. Commun.* pp. 83–84.
Sheldrick, G. M. (2008). *Acta Cryst.* A**64**, 112–122.
Spek, A. L. (2009). *Acta Cryst.* D**65**, 148–155.
Zheng, N., Zhang, J., Bu, X. & Feng, P. (2007). *Cryst. Growth Des.* **7**, 2576–2581.